Hydrogeology Journal (2018) 26:2283–2295
https://doi.org/10.1007/s10040-018-1754-x

REPORT

Assessment of key transport parameters in a karst system under different dynamic conditions based on tracer experiments: the Jeita karst system, Lebanon

Joanna Doummar[1] · Armin Margane[2] · Tobias Geyer[3] · Martin Sauter[3]

Received: 12 September 2017 / Accepted: 2 March 2018 / Published online: 28 March 2018

Abstract
Artificial tracer experiments were conducted in the mature karst system of Jeita (Lebanon) under various flow conditions using surface and subsurface tracer injection points, to determine the variation of transport parameters (attenuation of peak concentration, velocity, transit times, dispersivity, and proportion of immobile and mobile regions) along fast and slow flow pathways. Tracer breakthrough curves (TBCs) observed at the karst spring were interpreted using a two-region nonequilibrium approach (2RNEM) to account for the skewness in the TBCs' long tailings. The conduit test results revealed a discharge threshold in the system dynamics, beyond which the transport parameters vary significantly. The polynomial relationship between transport velocity and discharge can be related to the variation of the conduit's cross-sectional area. Longitudinal dispersivity in the conduit system is not a constant value ($\alpha = 7$–10 m) and decreases linearly with increasing flow rate because of dilution effects. Additionally, the proportion of immobile regions (arising from conduit irregularities) increases with decreasing water level in the conduit system. From tracer tests with injection at the surface, longitudinal dispersivity values are found to be large (8–27 m). The tailing observed in some TBCs is generated in the unsaturated zone before the tracer actually arrives at the major subsurface conduit draining the system. This work allows the estimation and prediction of the key transport parameters in karst aquifers. It shows that these parameters vary with time and flow dynamics, and they reflect the geometry of the flow pathway and the origin of infiltrating (potentially contaminated) recharge.

Keywords Tracer tests · Two-region nonequilibrium model · Karst · Lebanon

Introduction

At a catchment scale, conventional karst aquifers consist of a conduit network draining a fissured matrix with a potentially thick unsaturated zone frequently exceeding 100 m (Perrin et al. 2003). Karst conduits range between submeter diameters up to several meters in diameter. Furthermore, karst systems are characterized by both diffuse and point source infiltration mostly through fast flow pathways such as dolines (Kiraly 2002). As such, this duality of recharge and flow adds to the complexity of these systems. While large amounts of contaminants may be carried through the conduit at high velocities with limited sorption and degradation (Morales et al. 2007), pollutants can also migrate at relatively slower transit times through the different compartments of the karst system (i.e., fast infiltration points, epikarst, thick unsaturated zone, fissured matrix) before they finally reach the conduit network (Kogovsek and Petric 2014).

Artificial tracer tests are frequently employed to investigate rapid transport in karst from a potential source of pollution via the unsaturated zone and a conduit network system (Birk et al. 2005; Ford and Williams 2007; Göppert and Goldscheider 2008; Morales et al. 2010; Perrin and Luetscher 2008). The

✉ Joanna Doummar
jd31@aub.edu.lb

[1] Department of Geology, American University of Beirut, PO Box: 11-0236/26, Beirut, Lebanon

[2] Bundesanstalt für Geowissenschaften und Rohstoffe (BGR), Hannover, Germany

[3] Geoscientific Centre, University of Göttingen, Goldschmidtstr. 3, 37077 Göttingen, Germany

analysis of tracer breakthrough curves (TBCs) allows the quantitative assessment of the transport characteristics (transport velocities and dispersion) as well as their variation along a certain flowpath in a karst system (Field and Nash 1997; Perrin and Luetscher 2008). The resulting tracer breakthrough curve at the spring is revealed to be highly dependent on the geometry and hydraulic properties of the infiltration pathway (Kogovsek and Petric 2014). Many authors have shown that conduit geometries can be inferred from TBCs (Hauns et al. 2001; Perrin and Luetscher 2008) and that dispersivity increases with distance (Hauns et al. 2001; Seiler et al. 1989). Additionally, the analysis of artificial tracer tests yields information about transport processes of dispersion and advection, dilution, flow divergence and convergence (Smart 1988; Massei et al. 2006; Morales et al. 2007, 2010). Furthermore, some studies have used tracer test results to establish a correlation between tracer concentrations and peak transit time to define the type of flow in karst conduits (Jobson 1997; Morales et al. 2007).

Tracer breakthrough curves are usually analyzed using a conventional advection dispersion model (ADM); however, when ADM models fail to reproduce the skewness observed in the TBC, nonequilibrium models may be applied to account for the tailing effect resulting from exchange between mobile and immobile fluid regions (Field and Pinsky 2000; Geyer et al. 2007; Maloszewski et al. 1992; Morales et al. 2010). Nevertheless, the analysis of a single TBC with the nonequilibrium model might yield different sets of calibration parameters; therefore, the repetition of the tracer test allows not only assessment of the variation of transport parameters in karst conduits under different flow conditions (Göppert and Goldscheider 2008; Massei et al. 2006) but also helps refine model uniqueness. Additionally, transport in a karst environment is highly dependent on time and flow dynamics (Butscher and Huggenberger 2009; Doummar et al. 2014). Furthermore, the performance of tracer experiments in different injection points provides insight into the variability of transport parameters within the different compartments of a karst system (saturated versus unsaturated zones).

The present work aims at the assessment of conservative transport parameters through different compartments in a karst system from multiple TBCs observed at a spring. The results are compared, contrasted, and related to flow conditions and transport processes such as dilution, dispersion, and matrix-conduit tracer exchange (Smart 1988; Field and Nash 1997). For this purpose, 29 tracer experiments were conducted in a mature karst system in a semi-arid region (Lebanon), whereby, conservative tracers were injected in a phreatic conduit and in karst surface features. The recorded TBCs were systematically analyzed with a two-region nonequilibrium approach (2RNEM) to account for the observed skewness and pronounced tailing.

Study area

The tracer tests were carried out in the karst aquifer catchment of the Jeita spring, which is located north of Beirut in the Jounieh area in Lebanon. It constitutes the main domestic water source for the Beirut area and its northern suburbs (ca. 1.5 million inhabitants). Discharge of the Jeita spring ranges from 1.0 m^3/s during low flow periods to about 25 m^3/s during flood periods mostly as a response to precipitation events (based on continuous monitoring since 2009). Jeita Spring drains a catchment ranging in elevation from 90 to 2000 m above sea level (asl), and extending east into the Lebanese Mountains (Fig. 1). The lithology consists mainly of limestone and dolostone of Jurassic age overlain by formations of Middle to Upper Cretaceous age (sandstone, limestone, and marls). The catchment delineated using tracer experiment results, topographic heights, and lithostratigraphic contact boundaries, has an area of approximately 150 km^2.The Dog River, an ephemeral river, constitutes a no-flow boundary south to the catchment.

The total annual precipitation (rain and snow) in the Jeita catchment is estimated at approximately 1,200 mm on average (2009–2016; stations located at 950 and 1,700 m asl belonging to the Department of Geology, American University of Beirut, and at 14 m asl at Beirut International Airport). The spring constitutes the main outlet of the Jeita cave, which acts as an underground drainage channel developed in Jurassic limestone and dolomitized limestone. The total length of the surveyed cave (excluding tributaries) is ca. 5,300 m (Karkabi 1988) from the last accessible point to the cave outlet. Spring water is treated against bacteriological contamination before it is sent into the Beirut supply network; thus, there is an urgent need to understand the variation of conservative transport parameters under dynamic flow conditions for contamination management purposes. Point sources of pollution include hospitals, gas stations, slaughter houses, nontreated domestic waste water effluents and open solid waste dumps. Sampling has revealed the presence of persistent micropollutants, such as carbamazepine among others, in the epikarst during high flow (Doummar et al. 2014).

Materials and methods

Field experiments

Two artificial tracers, uranine (sodium fluorescein, BASF, CAS 518–47-8, $C_{20}H_{10}O_5Na_2$), and sodium naphthionate (CAS 130–13-2, $C_{10}H_8O_3NSNa$) were selected, since they are generally considered conservative and nontoxic below specific concentrations (Käβ 1998; Stockton et al. 2011). Concentrations of both tracers were monitored simultaneously

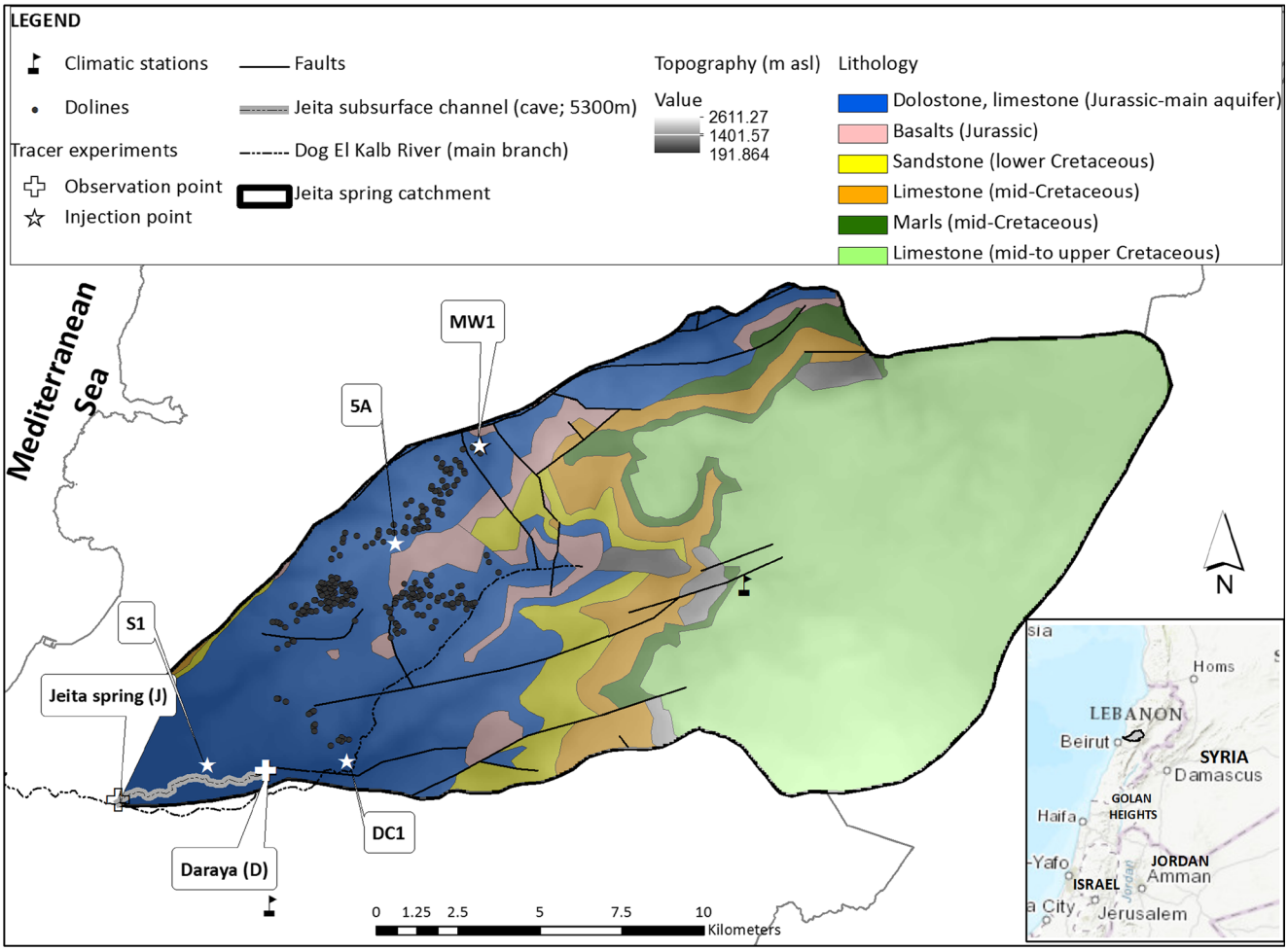

Fig. 1 Lithology and locations of tracer injection test sites conducted in the Jeita Spring catchment, N. Lebanon

in the spring using automatically logging (intervals of 15 min) field fluorometers (GGUN-FL30; Schnegg 2002). The field fluorometers were calibrated before every experiment with spring water and known solutions of the applied tracers according to the instrument calibration protocols (Schnegg 2002). The limit of detection of the field fluorometer is 0.02 μg/l for uranine, and 0.07 μg/l for sodium naphthionate. Flow rates were estimated based on monitored water level (20-min interval) based on a water level-flow calibration curve.

Between April 2010 and December 2011 a total of 29 artificial tracer tests were conducted in the Jeita spring catchment (Doummar et al. 2012), whereas 22 tracer injections were performed directly in the Jeita subsurface channel under different flow conditions.

Artificial tracers were also injected in two sinkholes (Fig. 1; S1 and 5A), an artificial pit hole (Fig. 1; DC1) and a borehole (Fig. 1; MW1) to acquire transport parameters within the unsaturated zone (fast and slow pathways) and in the fissured matrix before the tracer reaches the subsurface channel. Field fluorometers were deployed at the Jeita spring (J) at the main entrance of the subsurface channel (cave) for all the tracer tests, as well as at the end of it (end of the phreatic cave; D) for surface tracer tests. Details about mode of injection and injected masses are presented in Table 1.

Modeling technique

Key transport parameters (time to peak concentration; t_{cp}, time of first arrival; t_f, peak concentration (C_p), as well as duration of recovery; Δt) were retrieved graphically from the TBCs. Additionally, the observed TBCs were analyzed numerically using the process-based model CXTFIT 2.1/ in STANMOD (Toride et al. 1999; Van Genuchten et al. 2012). TBCs were modeled using a two-region nonequilibrium model (2RNEM) based on the assumption that the tracer migrates within a mobile fluid region and exchanges with an immobile fraction, stored in dead-end passages and pools from where it is slowly and gradually released back into the main conduit (Field and Pinsky 2000; Geyer et al. 2007, Göppert and Goldscheider 2008;

Table 1 Injection protocol and infiltration mode for surface and subsurface tracer experiments

Tracer experiment	Karst compartment	Injection protocol and infiltration of tracer
Conduit injections	Conduit	Instantaneous injection of a specific mass of uranine diluted in 20 l of spring water into D (access to the conduit 5,300 m upstream to J through a 500-m tunnel drilled in the valley)
S1	Sinkhole (22 m deep), fast flow pathway	Instantaneous injection of a mass of 5,000 g diluted in 50 l of water flushed pre- and post-injection with 20,000 l of water (injection time = 25 min)
5A	Sinkhole (depth unknown), fast flow pathway	Instantaneous injection of a mass of 9,373 g diluted in 50 l of water flushed pre- and post-injection with 60,000 l of water (injection time = 50 min)
DC1	Drilled pithole in unconsolidated alluvial deposits alongside the river, unsaturated zone	Instantaneous injection of a mass of 5,000 g diluted in 50 l of water flushed pre- and post-injection with 20,000 l of water (injection time = 60 min)
MW1	A supply well (350 m deep), fissured matrix	Instantaneous injection of a mass of 10,000 g of uranine diluted in 50 l of water directly into the well

Hauns et al. 2001). The delayed exchange between the mobile and immobile fluid region appears in the breakthrough curve as a dispersion effect and therefore reproduces the strong asymmetric tailing of a TBC, which cannot be reproduced with a simple ADM approach. The modeling of the TBCs with 2RNEM allows the estimation of mean tracer velocity (v_m), longitudinal dispersion (D), the assessment of the portion of immobile region, and the exchange coefficient between immobile and mobile regions. Reactive transport, i.e., decay and retardation, is not accounted for here, as it is regarded as negligible since only conservative tracers were used; therefore, the simplified governing equation for the 2RNE model is modified from Toride et al. (1999) as follows (Eqs. 1 and 2).

$$\beta\frac{\partial c_m}{\partial t} = D\frac{\partial^2 c_m}{\partial x^2} - v_m\frac{\partial c_m}{\partial x} - \omega(c_m - c_{im}) \quad (1)$$

$$(1-\beta)\frac{\partial c_{im}}{\partial t} = \omega(c_m - c_{im}) \quad (2)$$

where v_m is the mean velocity [L/T], D is the dispersion coefficient of the mobile region [L^2/T], β is the coefficient of partitioning between immobile and mobile fluid regions [−], ω is the first order mass transfer coefficient [1/T], c_{im} and c_m are the respective concentration of immobile and mobile fluid regions [M/L^3], x is the space coordinate [L] and t is time [T].

Tracer injection is assumed to be a Dirac pulse, i.e., instantaneous injection. The estimation of transport parameters with CXTFIT is performed inversely, based on initial transport parameters, to reproduce an observed tracer breakthrough curve.

An initial estimate of recovered mass M_R (in grams) was calculated by integrating tracer mass flux over the recovery duration (Eq. 3). The recovered mass was considered a fitting parameter estimated from the modeled TBC using Eq. (3).

$$M_R = \int c_i(t)Q_i(t)dt \quad (3)$$

where M_R is the recovered mass, c_i is the observed concentration and Q_i is the measured flowrate.

Based on the calibrated parameters, an equivalent phreatic flow cross-sectional area (A) averaged over the entire transport length using the total volume elapsed during the mean transit time divided by the total length (5,300 m) of the channel (Eq. 4) or the distance of transport D in the case of surface injections.

$$A = \frac{Q}{v_m} \quad (4)$$

where A is the phreatic flow area [L^2], Q the discharge during the time of recovery [L^3 T^{-1}], v_m the mean velocity [L/T] (Field 2002) for Q and v_m being considered as constant during the same tracer experiment based on a 30-min monitoring of water level and discharge. It is to be noted that this assumption is valid even during high-flow or event periods since mean transit times and duration of the breakthrough do not exceed 3 h. Longitudinal dispersivity (α in meters) was estimated from the ratio of calibrated longitudinal dispersion to mean velocity ($\alpha = D_L/v_m$) assuming no molecular diffusion due to the large scale of the experiments.

The model was calibrated by fitting all four parameters (v_m, D_L, β, and ω) one at a time, using two objective functions: the mean square error (MSE in µg/l; Eqs. 5 and 6) and the coefficient of correlation (R^2). A sensitivity analysis was performed to outline the most sensitive parameters

among the four. Mean velocity (v_m) and the coefficient of partitioning between mobile and immobile fluid regions (β) appeared to be highly sensitive (Geyer et al. 2007)

$$\mathrm{MSE} = \frac{1}{n}\sum_{i=1}^{n}(c_i - c)^2 \quad (5)$$

$$R^2 = 1 - \frac{\sum(c_i - c)^2}{\sum\left(c_i - \frac{1}{n}(\sum c_i)\right)^2} \quad (6)$$

where n is the total number of observation data, c_i is the observed concentration, and c is the modeled value.

Results and discussion

Through an extensive analysis of the TBCs, different transport parameters are respectively attributed to various karst compartments under different flow regimes in the subsurface channel, fast and slow flowing unsaturated zone (UZ), and fissured matrix and under mixed conditions (UZ and subsurface channel) in a karst system. Model parameters calibrated for tracer tests under different flow periods and injection conditions were correlated for a better understanding of rapid transport in karst systems under dynamic flow conditions. The relatively low mass recovery is explained by the large size of sinkholes and storage of the tracer in the relatively thick poorly wetted unsaturated zone, preventing optimal flushing conditions especially during low-flow periods. A lower mass recovery in the subsurface channel can also be attributed to a dampening of the fluorescence signals by the substantial turbidity characteristic of flood events. The TBCs obtained for tracer experiments conducted in the subsurface channel and in the surface features are presented normalized with respect to the peak concentration for comparison purposes (C_p; Fig. 2). The modeling results are shown in Tables 2 and 3.

Transport in the channel

Velocities, concentrations, flow areas, and transit times

The tracer breakthrough curves (TBCs) obtained from 22 artificial tracer experiments in the underground channel display only a slight tailing. Mean velocity estimated for discharge rates varying between 1.00 and 18.5 m^3/s ranges respectively between 0.08 and 0.53 m/s respectively. Similar velocities are characteristic of conduit flow and surface water flow (Morales et al. 2007). The velocity in the channel is not linearly correlated to the discharge rate, implying a variation in the wetted cross-sectional area, under different flow conditions (Fig. 3; Smart 1988). The wetted equivalent phreatic flow area A (Eq. 4) averaged over the entire distance (5,300 m) varies proportionally but not linearly with increasing discharge rate. The transit-time/discharge relationship over the distance of the subsurface channel (5,300 m) can be described by a power function (Fig. 3).

The relationship between t (mean transit time t_m) and time of first arrival (t_f) can be described by $t_m = 1.2\ t_f$, while, the relationship between the time to peak concentration (t_{cp}) and the time of first arrival (t_f) is as follows: $t_{cp=}\ 1.17\ t_f$. The three key times (t_{cp}, t_f, and t_m are correlated with spring discharge with different power functions (Table 4; Fig. 4a). Recovery times, i.e., duration of tracer breakthrough (Δt; time lapse between t_f and the time when concentration gets below detection limit) for the TBCs ranged between 0.6 and 6.2 h, which is a function of discharge ($\Delta t = 6.34Q^{-0.597}$; $R^2 = 0.8741$),

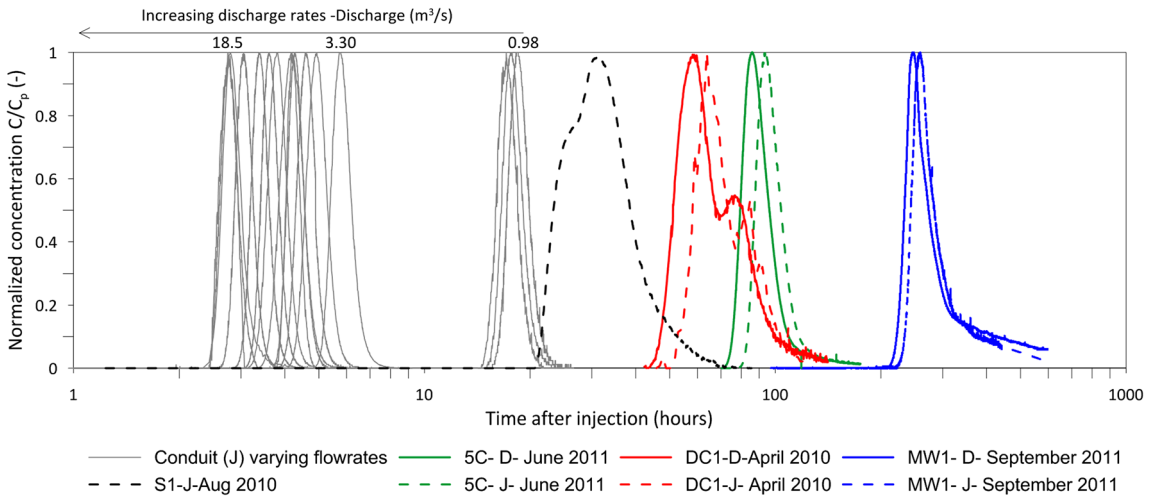

Fig. 2 Measured normalized TBCs (C/C_p) for the subsurface channel (5,300 m) and for surface injection, as a function of time after injection ($\log_{10}$ scale). For surface injections (S1, 5A, DC1, and MW1), recorded TBCs are observed at the main spring J (spring outlet) and at D (the beginning of the subsurface conduit)

Table 2 Graphical and model results of the tracer test experiments in the subsurface channel and karst subsurface features

Given										Graphical interpretation				2NREM fitting parameters			
Type	Name	Injection points	Observation point	Date (m/d/y)	Test No.	Tracer	M [g]	x [m]	Q [m^3/s]	C_p [10^{-3} g/m^3]	t_f [h]	t_{cp} [h]	Δt [h]	v_m [m/s]	D_L [m^2/s]	β –	ω [1/s]
Jeita Subsurface Channel (5,300 m)- Daraya			Jeita	9/15/11	1	Uranine	20	4,300	1.3	3.34	8.3	10	3.8	0.122	0.4	0.960	1.20E-07
			Jeita	8/17/10	2	Uranine	10	4,620	1.19	0.31	8.4	10	3.92	0.12	0.93	0.957	1.90E-08
			Jeita	9/15/11	3	Uranine	20	4,704	1.33	2.13	9.6	11	4.69	0.117	0.46	0.960	9.30E-08
			Jeita	8/17/10	4	Uranine	10	4,800	1.41	0.42	9.3	11	4.15	0.116	0.69	0.960	7.30E-08
			Jeita	12/4/10	5	Uranine	10	5,300	0.98	0.8	16	18	8.96	0.079	0.49	0.953	9.90E-08
			Jeita	11/24/10	6	Uranine	10	5,300	1.02	0.96	15	17	8.63	0.082	0.38	0.934	1.70E-07
			Jeita	11/10/10	7	Uranine	14	5,300	1.1	1.7	15	17	7.47	0.085	0.46	0.934	2.00E-07
			Jeita	9/15/11	8	Uranine	20	5,300	1.58	1.81	11	13	5.75	0.114	0.66	0.960	7.70E-08
			Jeita	7/13/11	9	Uranine	14	5,300	2.44	1.15	8.3	10	4.2	0.146	1.11	0.998	1.90E-09
			Jeita	12/21/10	10	Uranine	100	5,300	3.3	8.88	4.8	6	2.92	0.251	1.29	0.946	1.20E-07
			Jeita	2/9/11	11	Uranine	30	5,300	5.29	1.92	4.1	5	2.1	0.297	2.6	0.976	5.10E-08
			Jeita	2/20/11	12	Uranine	30	5,300	6.45	1.92	3.9	5	2	0.308	2.54	0.975	3.30E-09
			Jeita	2/6/11	13	Uranine	50	5,300	7.15	2.48	3.4	4	1.98	0.347	2.78	0.937	1.70E-07
			Jeita	3/6/11	14	Uranine	40	5,300	8.1	2.42	3.7	4	1.5	0.342	2.52	0.999	6.70E-10
			Jeita	2/17/11	15	Uranine	60	5,300	9	3.37	3.2	4	1.84	0.383	3.06	0.979	4.70E-08
			Jeita	3/16/11	16	Uranine	60	5,300	10.7	3.12	3.1	4	1.33	0.403	3.14	0.996	6.20E-08
			Jeita	3/11/11	17	Uranine	100	5,300	12	2.42	2.9	3	1.33	0.417	3.17	0.962	5.70E-09
			Jeita	2/22/11	18	Uranine	60	5,300	13.5	2.34	2.8	3	2.2	0.456	3.47	0.993	8.50E-09
			Jeita	2/28/11	19	Uranine	56	5,300	14.6	1.84	2.6	3	1.16	0.478	3.61	0.999	7.10E-10
			Jeita	1/31/11	20	Uranine	50	5,300	15.6	1.62	2.4	3	1.9	0.514	3.53	0.971	2.80E-08
			Jeita	2/27/11	21	Uranine	100	5,300	17.8	2.75	2.4	3	1.12	0.525	3.61	0.984	2.40E-08
			Jeita	2/21/11	22	Uranine	80	5,300	18.5	0.81	2.5	3	0.79	0.531	3.61	0.970	1.70E-07
Fast flow	S1	Sinkhole	Jeita	8/20/10	23	Naph	5,000	5,100	1.41	4.6	38	24	51	0.038	0.68	0.821	6.60E-08
	S1	Sinkhole	Jeita	8/21/10	23	Naph	5,000	5,100	1.41	6.07	25	30	51	0.056	1.18	0.990	2.80E-11
	5A	Sinkhole	Daraya	6/26/11	24	Uranine	9,373	7,000	2.08	15	70	87	94	0.022	0.19	0.917	6.80E-08
Mixed media	5A	Sinkhole	Jeita	6/26/11	25	Uranine	9,373	12,300	2.9	10.7	78	92	103	0.035	0.42	0.920	4.30E-08
	DC1	Pithole	Jeita	4/17/10	26	Uranine	5,000	7,500	3.35	1.28	46	68	68	0.03	0.81	0.869	3.10E-08
	MW1	Borehole	Jeita	9/16/11	27	Uranine	10,000	17,720	1.69	3.15	220	253	144	0.017	0.34	0.880	1.50E-08
Unsaturated zone	DC1	Pithole	Daraya	4/17/10	28	Uranine	5,000	2,700	2.4	1.6	43	47	51.2	0.013	0.2	0.800	6.60E-05
	DC1	Pithole	Daraya	4/17/10	28	Uranine	5,000	2,700	1.5	0.93	43	47	51.2	0.01	0.17	0.800	6.60E-05
Fissured matrix	MW1	Borehole	Daraya	9/16/11	29	Uranine	10,000	12,420	1.1	4.63	227	244	124	0.012	0.2	0.857	2.00E-08

M injected mass; x distance of transport; Q flowrate during experiment; *naph* sodium naphthionate; C_p peak concentration; t_f time of first arrival; t_{cp} time of peak concentration; Δt recovery time; v_m modeled mean velocity; D_L longitudinal dispersion; β coefficient of partitioning between immobile and mobile fluid regions; ω first order mass transfer coefficient t_m mean transit time (x/v_m); α longitudinal dispersivity; A phreatic area; M_R recovered mass; R^2 Coefficient of determination; *MSE* mean square error

Table 3 Calculated transport and geometry parameters from the model results and statistical evaluation of the model best fit. Coefficient of determination (R^2) and mean square error (MSE)

Given	Name	Injection points	Observation point	Test No.	Calculated					Statistics	
Type					t_m [h]	α [m]	A m^2	$M_{R\ (mod)}$ %	M_R/C_p (10^3m^3)	R^2 –	MSE [10^{-3} g/m^3]
Jeita Subsurface Channel (5,300 m)- Daraya			Jeita	1	10.00	3.3	11	100%	6	0.9999	1.00E-04
			Jeita	2	11.00	7.7	10	37%	12	0.9878	2.50E-04
			Jeita	3	11.00	4	11	77%	7	0.9992	4.00E-04
			Jeita	4	11.00	6	12	38%	9	0.997	4.80E-05
			Jeita	5	19.00	6.2	12	87%	11	0.9984	1.30E-04
			Jeita	6	18.00	4.6	12	100%	10	0.999	1.20E-04
			Jeita	7	17.00	5.4	13	100%	8	0.9959	1.40E-03
			Jeita	8	13.00	5.8	14	100%	11	0.999	3.80E-04
			Jeita	9	10.00	7.6	17	100%	12	0.9931	1.10E-03
			Jeita	10	6.00	5.1	13	98%	11	0.9996	3.60E-03
			Jeita	11	5.00	8.7	18	100%	16	0.9996	2.00E-04
			Jeita	12	5.00	8.2	21	100%	16	0.968	2.20E-03
			Jeita	13	4.00	8	21	100%	20	0.997	1.80E-03
			Jeita	14	4.00	7.4	24	100%	17	0.994	4.10E-03
			Jeita	15	4.00	8	23	100%	18	0.9995	6.30E-04
			Jeita	16	4.00	7.8	26	99%	19	0.9961	4.80E-03
			Jeita	17	4.00	7.6	29	43%	18	0.997	6.80E-03
			Jeita	18	3.00	7.6	30	87%	22	0.996	2.80E-03
			Jeita	19	3.00	7.6	31	73%	22	0.9958	1.80E-03
			Jeita	20	3.00	6.9	30	81%	25	0.9986	2.80E-04
			Jeita	21	3.00	6.9	34	71%	26	0.9955	3.50E-03
			Jeita	22	3.00	6.8	35	25%	25	0.9695	2.10E-03
Fast flow	S1	Sinkhole	Jeita	23	38.00	17.9	37	3%	28	0.9803	5.30E-02
	S1	Sinkhole	Jeita	23	25.00	20.9	25	7%	61	0.9415	1.40E-01
	5A	Sinkhole	Daraya	24	90.00	8.8	97	22%	138	0.996	6.00E-02
Mixed media	5A	Sinkhole	Jeita	25	98.00	12	84	23%	203	0.985	1.10E-03
	DC1	Pithole	Jeita	26	69.00	26.6	111	7%	267	0.9726	6.90E-03
	MW1	Borehole	Jeita	27	292.00	20.3	100	11%	363	0.99	7.40E-03
Unsaturated zone	DC1	Pithole	Daraya	28	59.00	15.8	189	5%	146	0.984	4.80E-03
	DC1	Pithole	Daraya	28	74.00	16.9	148	4%	199	0.985	1.10E-03
Fissured matrix	MW1	Borehole	Daraya	29	289.00	16.7	92	12%	250	0.9887	1.30E-02

t_m mean transit time (x/v_m); α longitudinal dispersivity; A phreatic area; M_R recovered mass; R^2 coefficient of determination; *MSE* mean square error

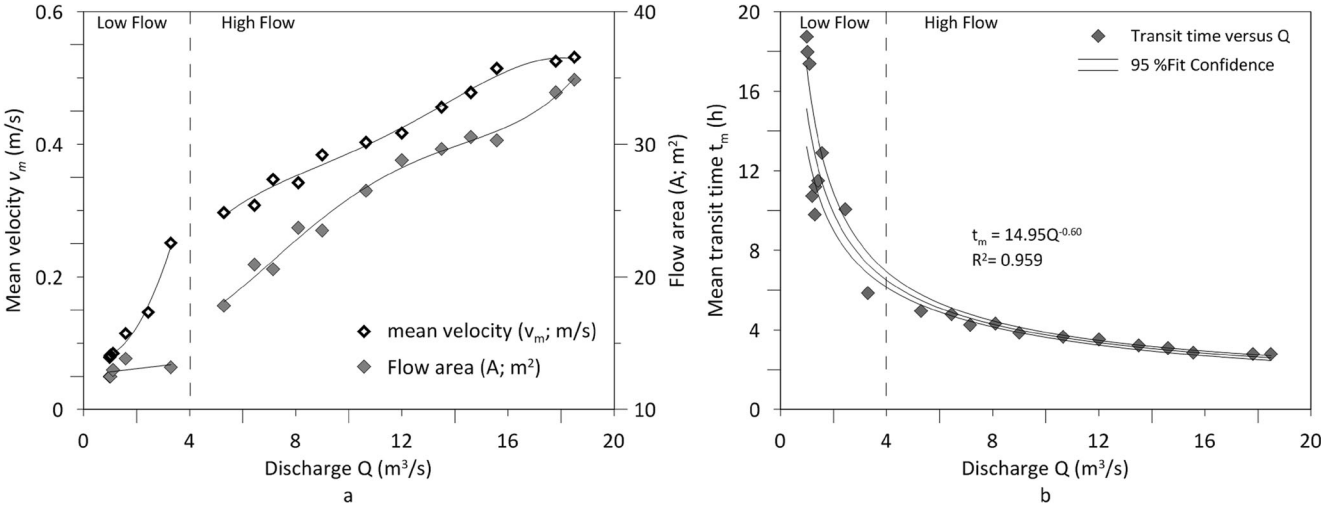

Fig. 3 Relationships between **a** mean velocity (v_m), average phreatic cross-sectional area (A) and discharge rate (Q), and **b** tracer mean transit time (t_m) and discharge (Q) in the subsurface channel

where Q is in m^3/s. The real time for recovery depends largely on the skewness of the TBC. According to this relationship between Δt and Q (Table 4), the calculated recovery time is slightly underestimated for low-flow periods due to the tailing effect.

The ratio of recovered mass to peak concentration is correlated to the discharge by a power function (Fig. 4b). Finally, peak tracer concentration to be expected during the time of recovery can be estimated based on the ratio of total recovered mass to total volume of dilution ($M_R/Q\Delta t$; Fig. 5a). For all flow periods, and any mass of conservative contaminant injected in the subsurface channel, maximum concentration (C_p), minimum recovery times (Δt), time of first arrival (t_f), mean time (t_m), and time to peak concentration (t_{cp}) can be calculated (Fig. 4; Table 4). R^2 values are considered satisfactory as they are close to 1 for almost all depicted relationships.

Longitudinal dispersion (D_L) and dispersivity (α)

Longitudinal dispersion (D) and mean velocity (v_m) increase with increasing discharge rate following a polynomial relationship ($R = 0.977$), implying that longitudinal dispersion does not vary linearly with velocity and that longitudinal dispersivity varies according to flow conditions in relation to conduit geometry. During high periods ($Q > 4$ m^3/s), the longitudinal dispersivity (α) shows a distinctive linear trend, i.e. it decreases linearly with increasing discharge rates ($\alpha = -0.115Q + 8.9$; $R^2 = 0.7802$; Fig. 6). During low-flow periods ($Q < 4$ m^3/s) this relationship does not apply, as longitudinal dispersivity (α) varies randomly between 3 and 8 m. Therefore, a constant dispersivity cannot be assigned to the channel under different flow periods as the dynamics appear to change above a certain threshold that appears to be related

Table 4 Table showing the relationship between key transport parameters and discharge in the subsurface channel (transit times, peak concentration, and duration of the tracer recovery) for a conservative tracer

Key transport parameters	Relationships (Q in m^3/s; Recovered mass in grams)	R^2
Subsurface channel		
Recovery time Δt (hours)	$\Delta t = 6.34\ Q^{-0.597}$	0.8741
Time to peak concentration t_{Cp} (h)	$t_{Cp} = 14.5\ Q^{-0.595}$	0.9568
Time of first arrival t_f (h)	$t_f = 12.3\ Q^{-0.591}$	0.9515
Mean time t_m (h)	$t_m = 14.9\ Q^{-0.600}$	0.9595
Mass and peak concentration	$Q = 0.0077\ (M_R/C_p)^{2.37}$	0.8771
Surface and subsurface		
Peak concentration C_p (10^{-3} g/m³ equivalent to µg/l)	$C_P = 0.996\frac{M_R}{Q\Delta t}$	0.7851
Time of recovery Δt (hours)-varying distance	$\Delta t = 0.0001\left(\frac{Q}{\alpha x}\right)^{-1.154}$	0.8043

Variables: Q discharge in m^3/s, α longitudinal dispersivity in m, M_R recovered mass in g, Δt recovery time in h, C_p peak concentration in 10^{-3} g/m^3, x distance of transport in m; t_{Cp} time to peak concentration in h, t_f time of first arrival in h, t_m mean transit time in h

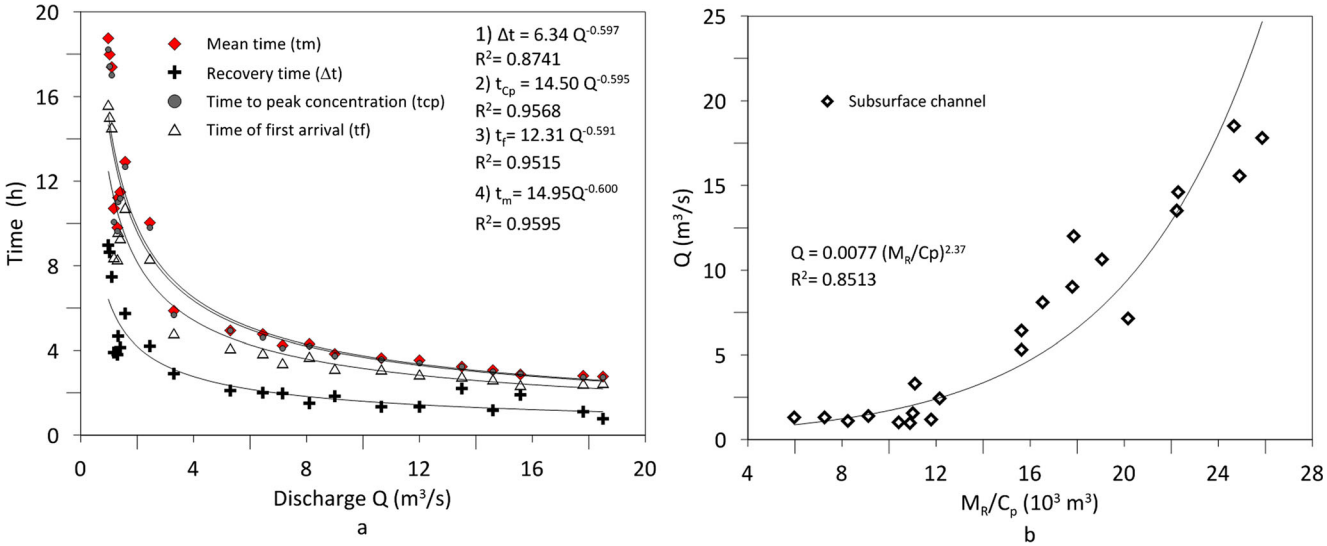

Fig. 4 **a** Relationship between Q (m^3/s) and key-times in hours: recovery time Δt, time of first arrival t_f, mean time t_m and time to peak concentration t_{cp}, and **b** relationship between flow (Q in m^3/s) and the ratio of recovered mass (M_R) to peak concentration (C_p)

to the sectional flow area. Furthermore, the recovery time (Δt) for tracer experiments in the subsurface channel over varying distances is closely correlated to the ratio of discharge and the product of dispersivity (α) and distance of transport (x; Table 4; Fig. 5b).

Immobile regions β and ω

The mobile fluid region coefficient (β) within the conduit ranges between 0.93 and 1.00 (Fig. 7) portrayed by a subtle tailing especially during low flow. The calibrated parameter β increases with increasing spring discharge, i.e., the percentage of stagnant flow regions within the conduit decreases with increasing flow velocities. Additionally, the larger the percentage of the immobile region ($1 - \beta$), the higher the exchange flux of tracer between the mobile and immobile region with time, displayed by the calibration parameter ω (Eq. 2; Fig. 7). This relationship, however, does not take into account exchange between the conduit and the matrix.

In the subsurface channel, transit times increase considerably once the discharge rate drops below 4 m^3/s. At the same discharge rate, a break in the longitudinal dispersivity and velocity series is observed, i.e. this discharge value can be considered as a threshold for a change in flow dynamics in the Jeita karst system. This discrepancy may be either attributed to a widening of the wetted area of the channel and/or to

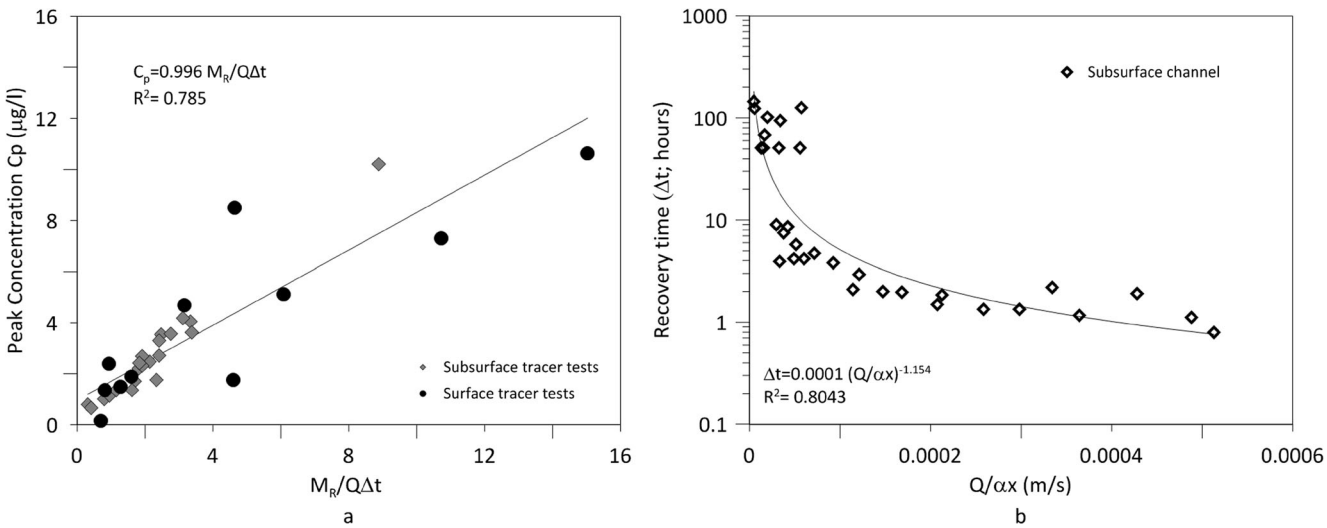

Fig. 5 **a** Relationship between peak concentration (C_p) and dilution, i.e., ratio of recovered mass (M_R in grams) to the product of discharge (Q in m^3/s) and recovery time (Δt in hours). **b** Relationship between recovery time (Δt) and ratio of discharge (Q in m^3/s) to the product of dispersivity (α in m) and transport distance (x in m) for both the subsurface channel and surface injections

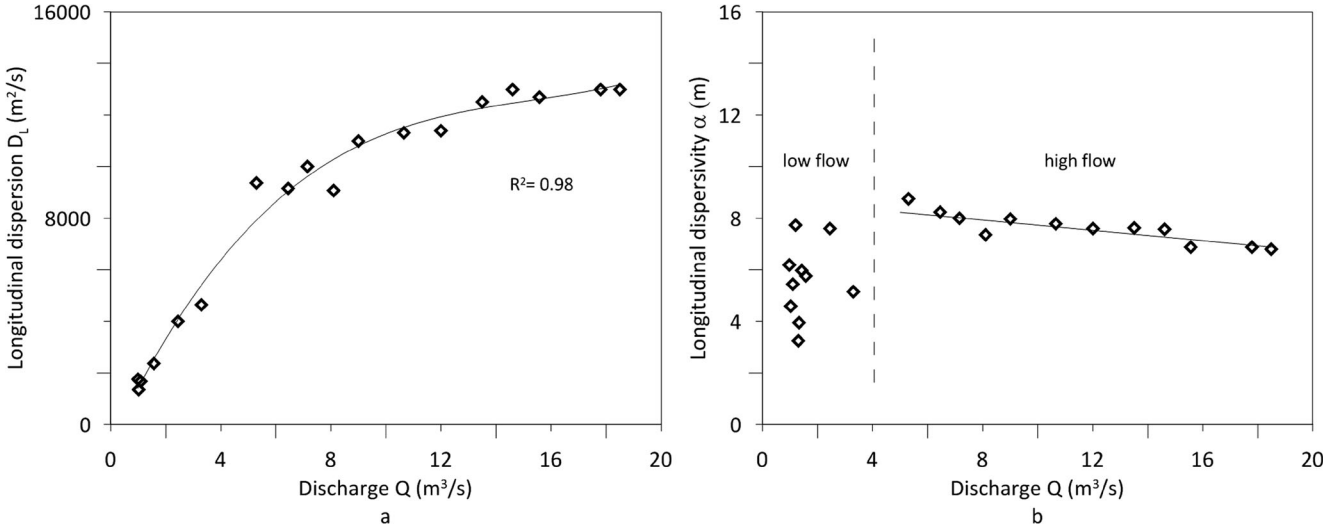

Fig. 6 Relationships between **a** longitudinal dispersion (D_L), **b** longitudinal dispersivity (α), and discharge (Q)

higher inflow from other conduit tributaries during precipitation events. TBCs during low-flow periods ($Q < 4$ m^3/s) generally display an asymmetrical shape where a longer tailing of the falling limb is observed. The strong tailing during low flow periods leads to a high variance with respect to a mean transit time in the TBC and is not due to dispersivity but to the higher proportion of immobile regions. The percentage of the mobile region contributing to the tracer breakthrough curve increases with decreasing velocity. The decrease in water level during low-flow periods and decrease of the wetted flow area lead to emergence of irregularities such as pools, riffles (abrupt changes in the channel slopes), and stagnant zones that enhance the proportion of the immobile region. The increase in turbulence with high flow velocities, and absence of irregularities in the subsurface channel during high flow periods, is believed to increase the tracer exchange flux between immobile and mobile flow regions thereby decreasing tailing effects.

The slight decrease in dispersivity during increasing discharge rate may be due to an increasing dilution effect from water inflowing to the channel during high-flow periods or to an increase in the efficiency of transport (Massei et al. 2006). During low-flow periods, longitudinal dispersivity is highly dependent on the degree of mixing of the tracer as well as the injection mode because partitioning between immobile and mobile zones becomes much more prominent under these conditions. Additionally, the large apparent longitudinal dispersivity and the relatively high transit times increase the duration of tracer recovery. From the transport parameters assessed for different discharge rates, a specific discharge

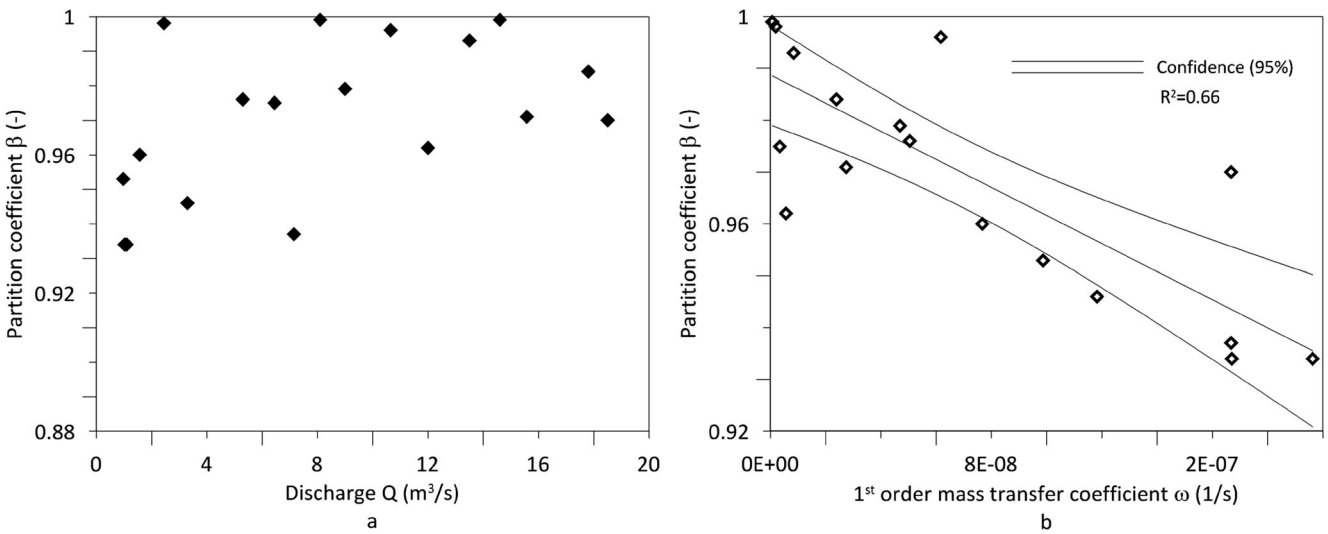

Fig. 7 Correlation between the **a** partitioning coefficient (β) and **b** discharge rate (Q), and the mass transfer coefficient (ω)

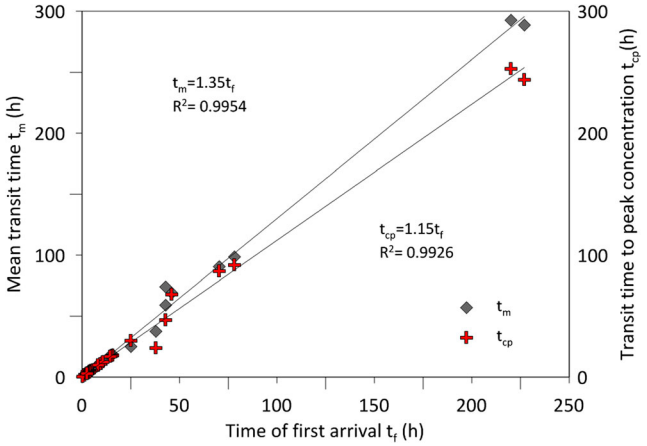

Fig. 8 Relationship between key transit times (mean transit time, time of first arrival and time to peak concentration) in the entire system including subsurface channels and karst compartments

threshold can be identified, beyond which the cross-sectional flow geometry and the hydraulic parameters the aquifer are believed to change.

Transport in the unsaturated zone and saturated matrix

As expected, tracer experiments with injection into a sinkhole at ground level (Fig. 1; 5A and S1), into a dug pit hole (Fig. 1; DC1) and a borehole (Fig. 1; MW1) display a somewhat different breakthrough pattern, as portrayed by the shape of the TBC, the greater tailing effects, the lower mass recovery, the more pronounced transit times, and the higher dispersivity values. The transport parameters are affected by the dispersion processes in the different compartments of the karst system such as the soil zone, epikarst, and unsaturated zone. This is reflected in the shape of the corresponding tracer breakthrough curves (i.e. for a tracer-transport experiment involving a vertical solution shaft, parameter values are very different from those estimated from experiments that involve a fissured matrix).

Tracer was injected at the surface injection points together with a considerable volume of pre- and post-flushing water. Therefore, it is not possible to assess to what extent saturated flow conditions prevailed in the thick unsaturated zone (200–400 m based on existing well records and geological cross sections), as the unsaturated zone changes the initial conditions and comparability between experiments.

Velocities and transit times

Calibrated mean flow velocities for the tracer experiments with surface injection features vary between 0.01 and 0.06 m/s, with lowest velocities reflecting transport in the fissured matrix; the highest values are typical for transport in sinkholes or vertical shafts linked directly to the karst conduit. Calculated flow velocities are much lower for tracer experiments with injections at the surface, reflected in long tracer residence times in the unsaturated zone. However, it should be noted that since the observed mean velocities depend on the injection mode and infiltration rate, they can therefore be regarded as maximum velocities, compared to conditions of natural infiltration.

Time to peak concentration and mean time can be estimated from time of first arrival in surface tracer experiments. They correlate well with data obtained from tracer

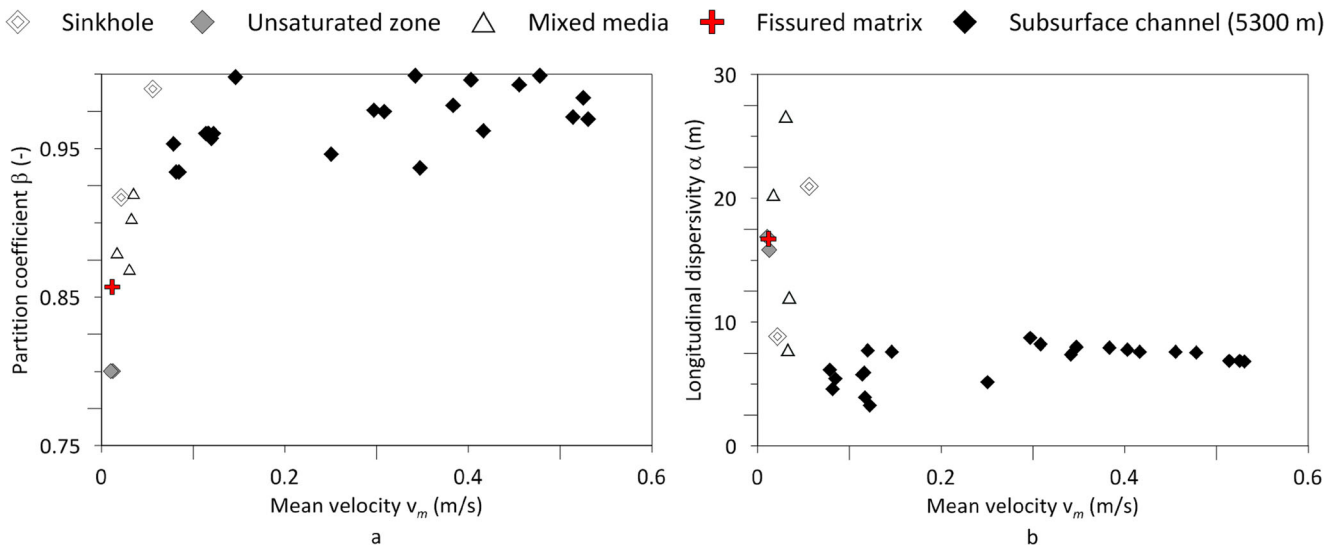

Fig. 9 Relationships between various transport parameters from 29 tracer experiments: **a** between mean velocity and partition coefficient (β); and **b** between mean velocity and longitudinal dispersivity

experiments with injection directly into the subsurface channel. The relationship between t (mean transit time t_m) and time of first arrival (t_f) can be described for the entire system (effects of subsurface channel and surface features) as follows: $t_m = 1.35\ t_f$ ($R^2 = 0.9550$), while the relationship between the time to peak concentration (t_{cp}) and the time of first arrival (t_f) is as follows: $t_{cp} = 1.15\ t_f$ ($R^2 = 0.9550$; Fig. 8). The expected peak concentration is also a function of ($M_R/Q\Delta t$) and follows the same relationship described earlier for the subsurface channel experiments (Tables 2 and 3; Fig. 5a).

Longitudinal dispersion and dispersivity

Tracer experiments with injections at the ground surface display longitudinal dispersivity values ranging between 8 and 27 m. These values are generally higher compared to those with direct injection into high-flow pathways (subsurface channel), i.e. the transport through the unsaturated zone leads to strongly increased longitudinal dispersivity.

The mobile region β estimated from TBCs in tracer tests conducted in surface features (sinkholes, pit holes, and the well) varies between 0.80 and 0.93 (Fig. 9). Lowest values of β are obtained for tracer tests with injection into pit holes, i.e., including transport in the unsaturated zone, as shown by the prominent tailing of the TBC, whereas the partition coefficient increases up to 1 for experiments where the injection sinkholes or shafts are linked to the main subsurface channel.

Three ranges of mean velocity are estimated based on the tracer experiments conducted with injection into karst surface features at ground level: mean velocities in the unsaturated zone (percolation through unsaturated fissured matrix blocks, around 0.01 m/s), mean velocities in sinkholes directly linked to the main sub-channel system (highest velocities: 0.06 m/s), and mean velocities which integrate both media. The fraction of the mobile region is lower for tracer experiments with injection into surface karst features (sinkhole, unsaturated zone; 0.80–0.92) and with respect to that in the subsurface channel (0.92–1.0). The latter suggests that the relevant tailing is generated before the tracer arrives at the subsurface channel. The increase in the partition coefficient with an increase in mean transport velocity shows that the greater the advective control in the tracer transport, the lower the proportion of immobile region, and tracer partitioning into mobile and immobile regions. Similar to transport in a channel, the recovery time for injections in surface features is correlated to the ratio of discharge to the product of longitudinal dispersivity and distance of transport (Tables 2 and 3; Fig. 5b).

Conclusions

An extensive campaign of tracer experiments unraveled the relationships among key transport parameters and their variation in a mature karst catchment area drained by the Jeita Spring (Lebanon). The TBCs were analyzed using 2RNEM to account for tailing generated in key parameters when studying karst aquifers. Relationships between discharge and other transport parameters (e.g., transit times, mean velocity, longitudinal dispersion and dispersivity, partition coefficient reflective of immobile regions, and peak concentrations) could be established under various flow periods. A different transport behavior is observed in the main draining conduit beyond a certain discharge threshold, indicating a change in the dynamics of the aquifer and, possibly, the cross-sectional flow area. Lower values of longitudinal dispersivity are observed during low discharge periods, yet the higher variance of the TBC with respect to a mean transit time is controlled by the immobile region (i.e., tracer partitioning and tailing), due to dispersive irregularities such as pools and riffles occurring with the lowering of the water level. On the other hand, longitudinal dispersivity is generally higher in high-flow periods above the discharge threshold because of increasing turbulence; however, it starts to decrease linearly with increasing flow rate probably owing to the effect of dilution.

This suggests that longitudinal dispersivity, which is usually regarded as a constant parameter of a system, effectively varies as a function of discharge and system geometry. Mean velocities observed in the unsaturated zone are in the range of 0.01–0.06 m/s. As expected, higher velocities are associated with sinkholes connected to the subsurface channel acting as fast flow pathways. Furthermore, if injection conditions are considered optimal, the analysis of TBCs in two different locations within the system indicates that most of the tailing due to immobile regions is mainly generated in the unsaturated zone and fissured matrix before the tracer reaches the main draining channel. This study highlights the variation of transport parameters under different flow conditions not only in the conduit but also in the different karst compartments. The latter gives insights into the efficiency of transport parameters in addressing specific vulnerability questions such as (1) time of first arrival, (2) recovery time, (3) mean transit time, (4) attenuation of peak concentration under varying flow conditions.

Acknowledgements Data were collected within the context of the cooperation project “Protection of the Jeita Spring” funded by the Bundesanstalt für Geowissenschaften and Rohstoffe (BGR; Germany) in Lebanon.

References

Birk S, Geyer T, Liedl R, Sauter M (2005) Process-based interpretation of tracer tests in carbonate aquifers. Ground Water 43(3):381–388

Butscher C, Huggenberger P (2009) Enhanced vulnerability assessment in karst areas by combining mapping with modelling approaches. Sci Total Environ 407(3):1153–1163

Doummar J, Margane A, Geyer T, Sauter M (2012) Protection of the Jeita Spring: tracer tests analysis. Special reports I–V. Protection of the Jeita Spring. Applied Geosciences. Georg August University, Göttingen, Germany

Doummar J, Geyer T, Baierl M, Nödler K, Licha T, Sauter M (2014) Carbamazepine breakthrough as indicator for specific vulnerability of karst springs: application on the Jeita spring, Lebanon. Appl Geochem 47:150–156

Field MS (2002) The QTRACER2 program for tracer-breakthrough curve analysis for tracer tests in karstic aquifers and other hydrologic systems. EPA/600/R-02/001. EPA, Washington DC

Field MS, Nash SG (1997) Risk assessment methodology for karst aquifers: estimating karst conduit-flow parameters. Environ Monit Assess 47:1–21

Field MS, Pinsky PF (2000) A two-region non equilibrium model for solute transport in solution conduits in karstic aquifers. J Contam Hydrol 44(1):329–351

Ford DC, Williams PW (2007) Karst geomorphology and hydrology. Chapman and Hall, London

Geyer T, Birk S, Licha T, Liedl R, Sauter M (2007) Multitracer approach to characterize reactive transport in karst aquifers. Ground Water 35(1):35–45

Göppert N, Goldscheider N (2008) Solute and colloid transport in karst conduits under low-and high-flow conditions. Ground Water 46(1): 61–68

Hauns M, Jeannin P-Y, Atteia O (2001) Dispersion, retardation and scale effect in tracer breakthrough curves in karst conduits. J Hydrol 241(3–4):177–193

Jobson H (1997) Predicting travel time and dispersion in rivers and streams. J Hydraul Eng 123(11):971–978

Karkabi S (1988) Coloration de la Riviere souterraine de Jiita et de la perte superficielle du Ouadi Nahr El Salib (Caza du Kesrouane) 1961–1971 [Tracer experiments in the Jiita underground river and in the sinking stream of Wadi Nahr El Salib (Keserwan District) 1961–1971]. Al Ouat'Ouate 3:80

Käβ W (1998) Tracing technique in geohydrology. Balkema, Rotterdam, The Netherlands, 589 pp

Kiraly L (2002) Karstification and groundwater flow. In: Proceedings of the conference on evolution of Karst: from Prekarst to cessation. Postojna-Ljubljana 155–190

Kogovsek J, Petric M (2014) Solute transport processes in a karst vadose zone characterized by long-term tracer tests (the cave system of Postojnska Jama, Slovenia). J Hydrol 519(part A):1205–1213

Maloszewski P, Harum T, Benischke R (1992) Mathematical modelling of tracer experiments in the karst of Lurbach system. Steirische Beiträge Hydrogeol 43:116–136

Massei N, Wang H, Field MS, Dupon JP, Bakalowicz M, Rodet J (2006) Interpreting tracer breakthrough tailing in a conduit-dominated karstic aquifer. J Hydrol 14:849–858

Morales T, Fdez I, Valderrama D, Uriarte JA, Antiguedad I, Olazar M (2007) Predicting travel times and transport characterization in karst conduits by analyzing tracer-breakthrough curves. J Hydrol 334:183–198

Morales T, Uriarte JA, Olazar M, Antigüedad I, Angulo B (2010) Solute transport modelling in karst conduits with slow zones during different hydrologic conditions. J Hydrol 390:182–189

Perrin J, Luetscher M (2008) Inference of the structure of karst conduits using quantitative tracer tests and geological information: example of the Swiss Jura. Hydrogeol J 16:951–967

Perrin J, Jeannin PY, Zwahlen F (2003) Epikarst storage in a karst aquifer: a conceptual model based on isotopic data, Milandre test site, Switzerland. J Hydrol 279:106–124

Schnegg PA (2002) An inexpensive field fluorometer for hydrogeological tracer tests with three tracers and turbidity measurement. In: Bocanegra E, Martinez D, Massone H (ed) Proc. of the XXX/IAH Congress Groundwater and Human Development. Mar Del Plata, Argentina, October 2002, pp 1484–1488

Seiler K-P, Maloszewski P, Behrens H (1989) Hydrodynamic dispersion in karstified limestones and dolomites in the upper Jurassic of the Franconian Alb, F.R.G. J Hydrol 108:235–247

Smart CC (1988) Artificial tracer techniques for the determination of the structure of conduit aquifers. Ground Water 26(4):445–453

Stockton KA, Moffitt CM, Blew DL, Farmer CN (2011) Acute toxicity of sodium fluorescein to ashy pebblesnails *Fluminicola fuscus*. Idaho Dept. of Water Resources,, Moscow, ID, 21 pp

Toride N, Leij FJ, van Genuchten MT (1999) The CXTFIT code for estimating transport parameters from laboratory or field tracer experiments, version 2.1. Res Rep 137, US Salinity Laboratory, Riverside, CA

Van Genuchten M, Simunek JJ, Leij FJ, Toride N, Miroslav S (2012) STANMOD: model use, calibration, and validation. Trans ASAE 55:1353–1366